

## The Electronic Structures and Bonding of Some Transition-metal Monoborides

David R. Armstrong and Peter G. Perkins

Department of Pure and Applied Chemistry, University of Strathclyde, Glasgow G1 1XL, Scotland

**Eugenio A. Cetina V.**

Instituto de Investigación en Materiales, U.N.A.M., Ciudad Universitaria, Mexico 20, D.F., Mexico

The band structures and densities of states for the isostructural monoborides of Ti, Mn, Fe, and Co have been calculated by a LCAO-TB method. These results are related to the physical and spectroscopic properties of the materials. A satisfactory account of the ESCA spectra and a qualitative correlation with the electrical and magnetic properties is afforded by the calculations. A second series of calculations by the periodic cluster method is also carried out in order to reveal more details of the bonding and the effects of diffusion of electrons into the unoccupied levels above the Fermi edge.

**Key words:** Transition metal monoborides—Band structure—Density of states—Cluster model—Bonding and diffusion of electrons.

### 1. Introduction

The borides are a class of compounds which show an array of stoichiometries and structures [11]. Moreover, their physical properties have made many of them of considerable technological interest. Despite this and the obvious rationale of their properties and the bonding in the crystals which could result from a theoretical approach, very little theoretical work has been performed on the structures. We have previously published calculations on hexaborides and diborides [1, 2, 3] and we now apply the method to a study of the more structurally complex monoborides of transition metals. We find in this way we can obtain a

satisfying rationale of the known electronic, spectroscopic, and magnetic properties of these materials. Furthermore, the nature of the bonding is illuminated and correlated with the known physical properties.

## 2. Method of Calculation

### 2.1. Crystal Structure

All the borides studied are isostructural and have the orthorhombic B-27 structure; this typified by FeB [11]. There are eight atoms per primitive unit cell.

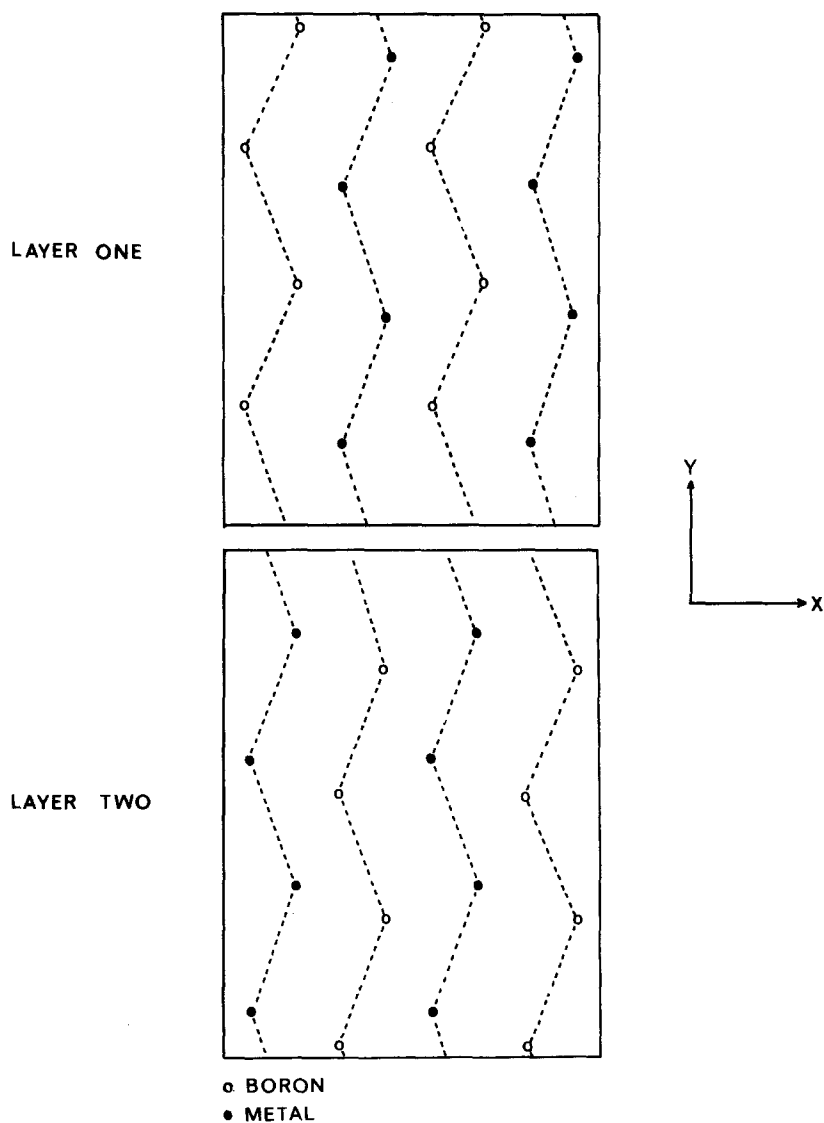
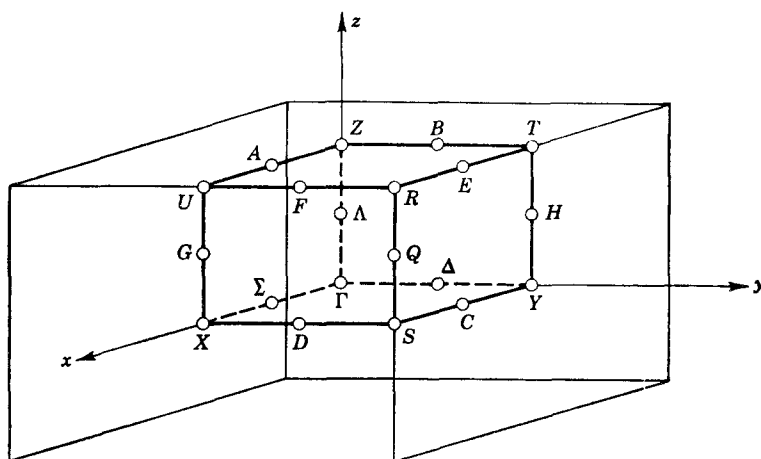


Fig. 1. Crystal Structure of Fe-B

**Table 1.** Lattice parameters and input atomic data for the monoborides

	Orbital exponent			VOIP (eV)			lattice constants of MB (nm)		
	<i>s</i>	<i>p</i>	<i>d</i>	<i>s</i>	<i>p</i>	<i>d</i>	<i>a</i>	<i>b</i>	<i>c</i>
Ti	1.075	0.725	2.280	6.07	3.35	5.58	0.4560	0.6112	0.3054
Mn	1.450	0.950	2.930	6.82	3.60	7.93	0.4145	0.5560	0.2977
Fe	1.575	1.025	3.150	7.07	3.72	8.68	0.4061	0.5506	0.2952
Co	1.700	1.100	3.367	7.31	3.84	9.42	0.3956	0.5243	0.3043
B	1.225	1.000	—	14.05	8.30	—	—	—	—

**Fig. 2.** Brillouin Zone for the Orthorhombic B-27 Structure

The structure is shown in Fig. 1 and in the crystal, the boron atoms form zig-zag chains in the *y*- and *z*-direction. The metal atoms have six boron neighbors and lie in site symmetry which is approximately octahedral. The lattice vectors for all the crystals are given in Table 1.

The Brillouin zone is also orthorhombic and its symmetry features are shown in Fig. 2.

## 2.2. Band Structures

Although the basic principles of the method stem from that employed previously [1–3], we have made some technical advances in its implementation, in particular in construction of the various density-of-states plots and the automatic analysis of the band symmetries. The method of calculation here adopted followed closely that discussed fully in a previous paper dealing with transition-metal monophosphides [13]. For brevity, we give no details here but refer the reader to that paper. The input atomic data for the calculations are given in Table 1.

In the present work, all principal symmetry lines of the Brillouin zone were included in the calculation and interactions with 890 neighbor unit cells were

incorporated. The density-of-states sampling was implemented as in Marwaha, Perkins, and Stewart (*op. cit.*)

### 2.3. Cluster Calculation

The method used for the superlattice cluster calculation has also been fully described [16] but, since the basis of this method is less well-known, we give a brief resumé here. A large superlattice cell containing several primitive cells is allowed to interact with a defined number of neighbors under Born–Von Kármán conditions. This is a pseudo-molecular calculation and yields eigenvalues, eigenvectors, an electron density matrix, and a *bond index* matrix [4]. The bond indices may be related directly to bond strengths [5]. One must choose a particular form of Hamiltonian in order to evaluate the intercell interactions and, in the present work, we adopted the Extended Hückel formalism [7]. This procedure was followed so that we could relate the cluster calculations to the present band-structure results.

In the cluster chosen, there were 16 metal and 16 boron atoms and these formed the supercell shown in Fig. 1. This cluster was allowed to interact with 225 neighboring supercells and the eigenvalue spectrum calculated. This shows closely spaced levels on the border of the occupied/unoccupied region (quasi-continuous in the band structure) and it is, clearly, of some interest to determine the effect of limited-energy electronic excitation on the nature of the bond in the crystal. The calculation was, therefore, modified in order to allow for “excitation” of electrons into adjacent vacant levels and recalculation of the bonding pattern. This simulates roughly the effects of temperature or of mutual electron repulsion (particularly when the paired electrons are localized on one atom). Two cases were studied, in which excitations 0.01 and 0.1 eV above the occupied level were envisaged.

## 3. Results and Discussion

### 3.1. Band-structure Features

Fig. 3 shows the band structure of FeB in all symmetry directions. The gross topological features of this diagram are common to all these isostructural borides and, hence, the detailed results for the others are not shown here. We report and comment in context on differences where they arise. The most immediately striking feature which is relevant to the bonding is the band widths. All the valence bands generated in the  $k_z$  direction ( $\Gamma$ -Z, T-Y, R-S, U-X) are broad, whilst those in the  $k_x, k_y$  plane are narrower. This indicates that the principal bonding interactions lie along the  $c$  direction in the crystal, those in other directions being more limited. The  $c$  direction in the crystal is the one in which lie both the zig-zag chains of B atoms which are mutually distanced by 1.78 Å (as in many of the diboride B nets) [11] and in which chains of metal atoms also lie. The chains are formed by atoms in layer one (Fig. 1) connected to those in layer two. The valence bands in the  $\Gamma$ -Z direction resemble those of AlB<sub>2</sub> in the

$\Gamma$ - $K$  direction. In the latter case, these bands bring about strong B-B bonding in a 2D hexagonal net. Hence, clearly, the B-B chain bonds are of considerable importance to the cohesion of the MB crystal. The presence of such strong anisotropy in the bonding is of some considerable interest. The pseudo-one-dimensional nature of the boron chain in these borides should provoke experimental interest in a further examination of the anisotropy of their properties. The conduction bands merge with valence band in all regions of  $k$ -space and the Fermi level is found in the narrow group of  $d$ -bands which lie in the center of

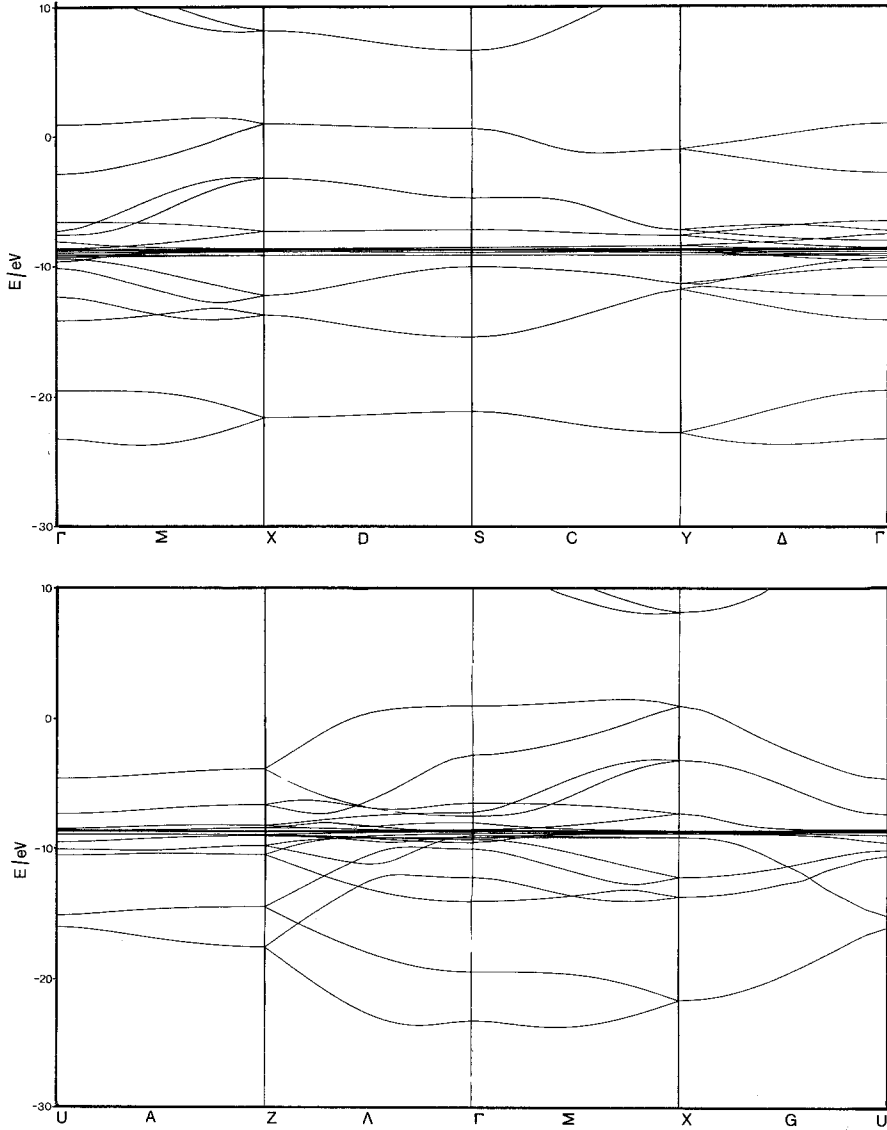


Fig. 3. Band Structure for FeB

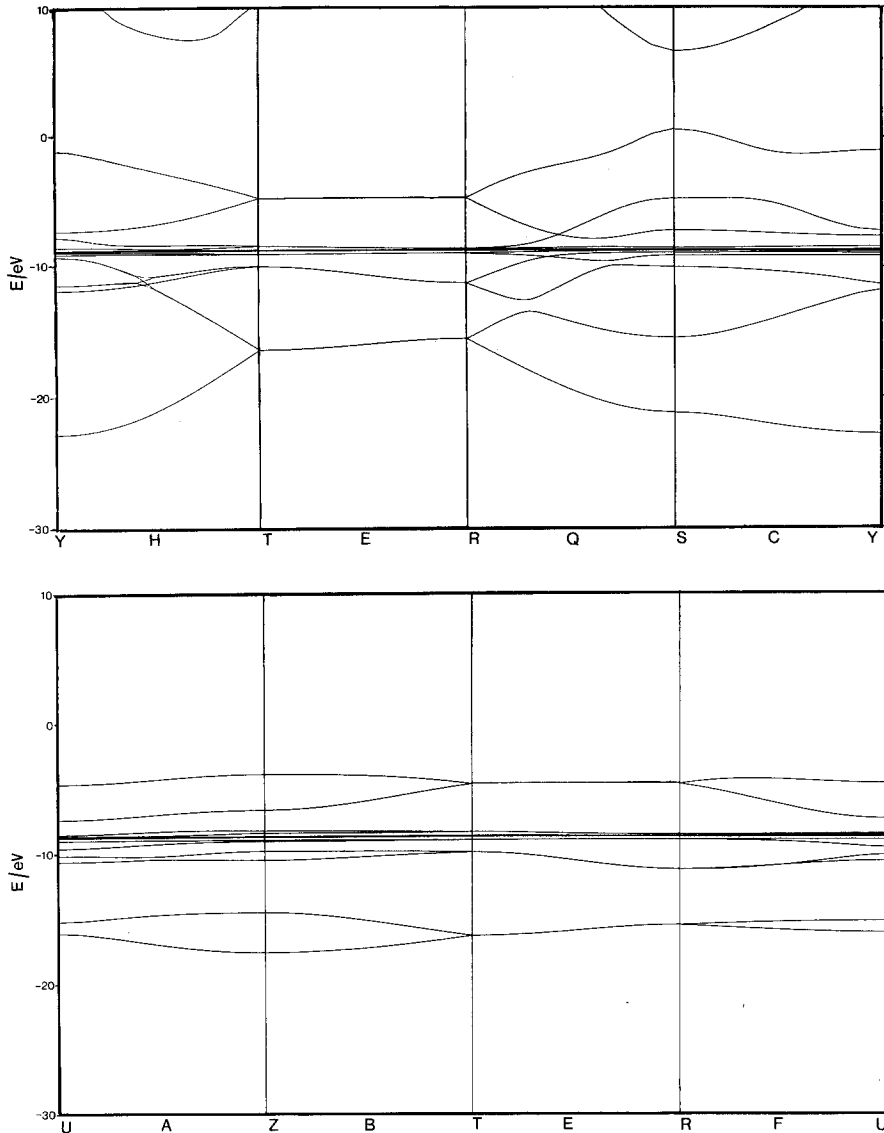


Fig. 3 (cont.)

the band diagram (*vide infra*). The conduction bands are less well characterised than the valence bands but it is clear that they are also somewhat broad in the  $z$ -direction and are consistent with the known metallic nature of the compounds [9].

### 3.2. Densities of states

The total density-of-states plots are shown in Fig. 4 for the series of borides. Fig. 5 shows the partial density of states for the boron states of FeB (typical for

the series) and Table 2 gives the detailed parentage of the bands of FeB at the  $\Gamma$  point. The total density-of-states plots show the calculated Fermi level. The lowest-lying bands in the energy scale originate from boron  $2s$  states, whilst the next group are the bonding Fe–B band. In the latter group, boron  $2p$  states are prominent. The large, narrow band (about 1.5 eV wide) in each total density-of-states plot consists predominantly of metal  $3d$  states. This latter narrow band

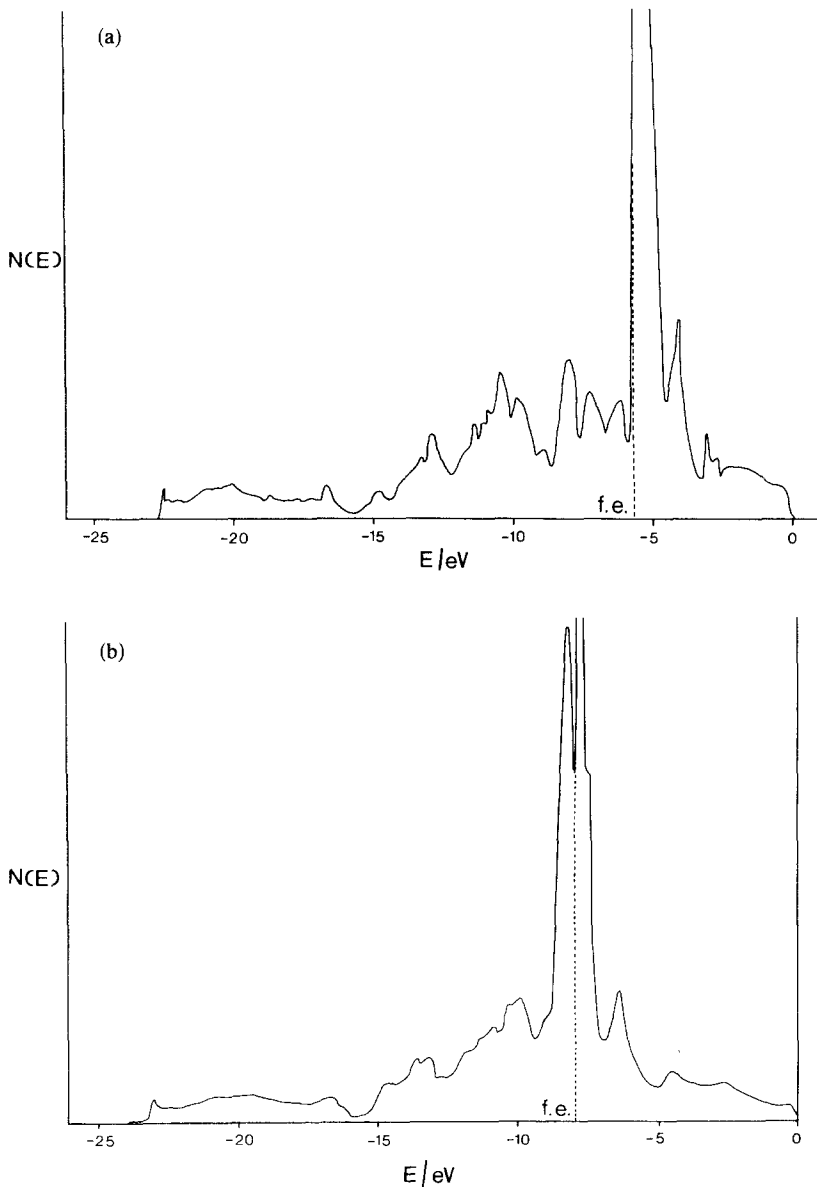


**Fig. 4.** Total Density of States for the Monoboride Series. (a) TiB, (b) MnB, (c) FeB. The experimental ESCA curve scaled from Ref. [9] is superimposed, and (d) CoB

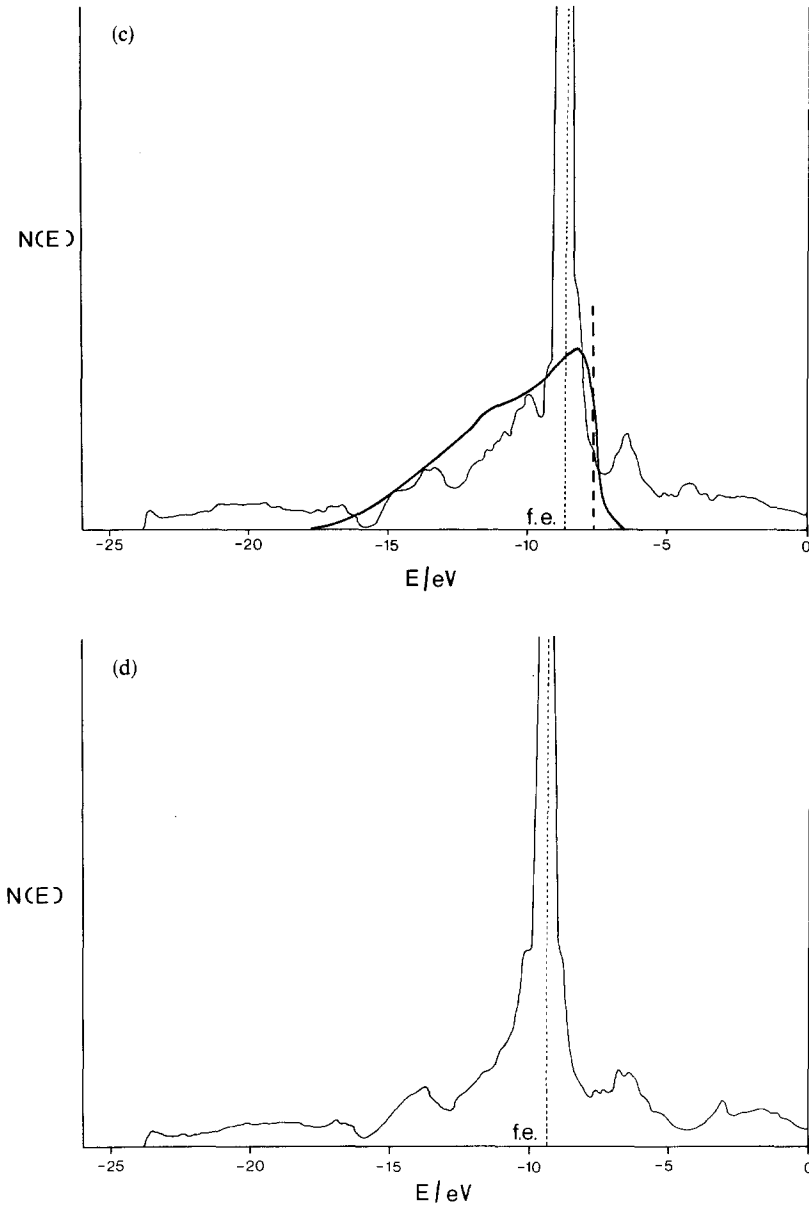


**Fig. 4** (cont.)

of states is strikingly similar to that calculated for binary transition-metal phosphides [13] and for transition-metal oxides [15]. It is also interesting that a portion (*ca* 20%) of boron  $2p$  states appears at and just above the Fermi level itself and these states have a spread of *ca* 0.5 eV.

Recently, a thorough study of the ESCA spectrum and derived properties of FeB has been undertaken by Joyner, Johnson, and Hercules [9, 10] and it is

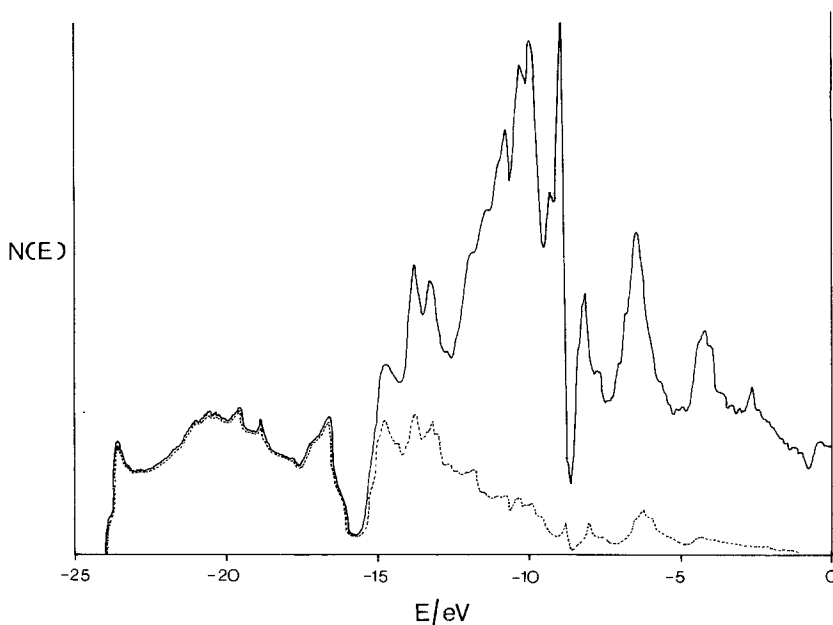


**Fig. 5.** Total Boron States and Partial Density of Boron  $2s$  States for FeB: Full line —,  $2p$  states; Broken line ---,  $2s$  states

relevant to compare our theoretical results with theirs. On Fig. 4c, we show the experimental ESCA curve for FeB superimposed on our total density of states for FeB. Although the Fermi levels do not coincide, we have lined up the two spectra so that their main features coincide. Our Fermi level appears to be only *ca* 0.75 eV lower in the absolute energy scale than theirs. The gross features of the experimental ESCA spectrum and the total density of states coincide, in that the experimental spectrum shows its highest maximum in the region of the Fermi level. This curve then descends towards the higher-binding-energy area in a manner parallel with that of the theoretical spectrum. It is clear, however, that the experimental spectrum (which, according to Joyner *et al.*, is composed only of iron  $d$  and  $s$  states) is rather broader than that calculated. The calculated  $d$  band appears to be too narrow and, if broadened, then the Fermi levels would coincide rather more precisely. In addition, the theoretical curve contains boron  $2p$  and  $2s$  states as well as, in the higher-binding-energy region, Fe  $s$  and Fe  $p$  states: these lie at binding energies in the region of 2–3 eV. Joyner *et al.* do not observe boron states but synchrotron photoemission studies in the photon energy range 25–180 eV [9, 10] have revealed boron states in FeB lying between binding energies of 5 and 15 eV. Our results concur very well with this observation and we can, moreover, supply a more detailed analysis. The onset of boron *bonding* states occurs at *ca* 0.5 eV below the Fermi level and a high count of  $2p$  states is evident between this point and *ca* 15 eV. The boron  $s$  states lie lower than this and, hence, we have good qualitative agreement with the synchrotron experiments. The presence of a significant density of boron  $2p$  states lying at

**Table 2.** Atomic Populations of Bands 1–27 of FeB at the  $\Gamma$ -point

Orbital	Energy (eV)	Atomic %B		Populations %Fe		
		<i>s</i>	<i>p</i>	<i>s</i>	<i>p</i>	<i>d</i>
1	-23.22	111.2	0.2	-10.9	-0.5	0.0
2	-19.50	93.1	7.5	2.7	-3.4	0.1
3	-14.10	6.8	80.5	21.6	-9.4	0.2
4	-12.24	17.8	62.9	2.2	13.9	2.9
5	-10.04	8.0	54.8	0.0	9.2	27.9
6	-9.56	0.3	50.3	6.8	31.1	11.0
7	-9.31	6.6	41.7	0.0	6.3	51.3
8	-9.19	0.0	23.7	2.7	4.4	69.2
9	-9.17	0.0	22.9	0.0	0.1	76.9
10	-9.01	0.0	63.1	0.0	9.1	27.9
11	-8.86	0.1	8.9	0.0	3.6	87.3
12	-8.72	0.0	0.7	0.0	0.1	99.2
13	-8.71	0.0	0.3	0.0	0.0	99.6
14	-8.71	0.0	0.2	0.0	0.0	99.8
15	-8.70	0.0	0.0	0.0	0.0	100.0
16	-8.70	0.0	0.2	0.0	0.2	99.6
17	-8.69	0.0	0.0	0.0	0.1	99.9
18	-8.69	0.0	0.0	0.0	0.4	99.6
19	-8.68	0.0	0.0	0.0	0.0	100.0
20	-8.68	0.0	0.0	0.0	0.0	100.0
21	-8.67	0.0	0.3	0.0	0.0	99.7
22	-8.67	0.0	0.0	0.0	0.0	100.0
23	-8.66	0.0	0.4	0.0	0.0	99.6
24	-8.66	0.0	0.0	0.0	0.0	100.0
25	-8.61	0.0	3.2	0.1	1.8	94.9
26	-8.54	0.0	23.0	0.0	4.3	72.7
27	-8.00	2.5	21.6	0.0	3.6	72.3

just above the Fermi level underscores the importance of these states for the electrical conductivity of the material. This means that the electrical conductivity should be pronouncedly anisotropic, having its maximum value along the strongly bonded boron zig-zag chains.

The position of the Fermi level in the series reflects the filling of the  $3d$  band and, over the series, the Fermi level descends in energy from Ti to Co. This parallels the trend in first ionisation potentials of the metals although, as seen above, in comparison with the experimental level for FeB, it is likely that the Fermi levels have been calculated only to 0.5–1 eV.

Since, as stated earlier, the metal atom lies in an approximately octahedral environment with respect to six boron atoms, then the  $3d$  band should, in principle, be split into two components corresponding to the molecular  $e_g$  and  $t_{2g}$  components of octahedral symmetry. However, this splitting is apparent only in the case of the manganese boride. Since each boron is bonded to other atoms in the crystal, they obviously do not afford such a strong crystal field as is found in a normal “molecular” transition-metal complex.

**Table 3.** The electron distribution of the monoborides obtained from the density-of-states calculation

	Boron Population		Charge	Metal Population			Charge
	<i>s</i>	<i>p</i>		<i>s</i>	<i>p</i>	<i>d</i>	
TiB	1.16	3.15	-1.31	0.33	0.22	2.15	+1.31
MnB	1.13	2.48	-0.61	0.35	0.25	5.79	+0.61
FeB	1.10	2.20	-0.30	0.35	0.13	7.22	+0.31
CoB	1.10	1.91	-0.01	0.36	0.14	8.49	+0.01

### 3.3. Charge Distribution

The density-of-states plots, on analysis, give rise to the atomic-orbital populations and the crystal polarity. Table 3 shows these data for this series of compounds. The positive charge calculated for the metal atom decreases regularly from Ti to Co and, as calculated, the material CoB is effectively non-polar. We expect this calculation to produce a rather exaggerated charge distribution, since no self-consistency was incorporated in the calculation. We believe that the trend in sign of the charges will be maintained, however. Hence, for the case of FeB, we expect the charge transfer to be given at a limit by the drift of 0.3 electrons from iron to boron. This is indeed small when one considers that, in this compound, the iron is formally  $\text{Fe}^{3+}$ . In keeping with this, Joyner *et al.* [9, 10] find from their study of the ESCA spectrum of FeB that the charge transfer  $\text{Fe} \leftrightarrow \text{B}$  is very small. It is clear from Table 3, over the whole series, that the metal *s* orbital is the one which loses a large proportion of its electrons and these are picked up by the *d* orbitals of the metal and, except for the case of CoB, by the *s* and *p* orbitals of the boron. The metal *d* electron populations are striking in that, in all cases, they exceed the formal atomic *d* orbital population of Ti  $d^2$ , Mn  $d^5$ , Fe  $d^6$ , Co  $d^7$ . The calculated *d*-orbital populations of the elements are in linear relationship with the formal number of *d* electrons and if the series is extrapolated to nickel ( $d^8$ ), then we obtain a *d*-orbital population for nickel of 9.8 *d* electrons, i.e., the *d* sub-band is virtually full. We correlate this later with the magnetic properties of NiB.

### 3.4. Electrical and Magnetic Properties

As stated above, the continuity of the valence and conduction bands renders these borides metallic. Of particular interest is the contribution of the boron  $2p$  states around the Fermi level and in the low-conduction levels. This means that electrons in the conduction band can be delocalised down the boron zig-zag chains and through the interstices of the lattice. Joyner *et al.* [9, 10] interpret the electronic conductivity of FeB as stemming from movement of conduction electrons through these interstices. Later, we analyze the nature and population of electrons which contribute in this way. The measured electrical conductivity of FeB in fact is substantial, being about 0.1 that of iron metal itself [9, 10].

Analysis of the magnetic properties of the monoborides is profitable and this is now considered. A method of partition of the *d* electrons on a transition-metal

atom according to whether they are “localized”, ‘itinerant’ or ‘conducting’ has been formulated [8] and for iron, the conclusion has been reached that there are six localized  $d$  electrons, 0.5 itinerant  $d$  electrons and 1.5 conduction electrons per iron atom which move in the interstices of the lattice. We can do an analysis of these groups of electrons for MB systems using the partial-density-of-states curves integrated between chosen energy points. Hence, for FeB, we derive the configuration as follows: the 7.22 Fe  $d$  electrons are first placed, two by two, in the three lowest  $d$  orbitals of the  $d$  band. This leaves 1.22  $d$  electrons to be distributed. The localized moment for FeB [12] is given as 1.09 Bohr magnetons and this can be accommodated by 1.155 electrons with spin-up and 0.065 electrons with spin-down. Hence, we can write  $(d^7)_1(d^{0.22})_i$ . Since the iron atom has a non-self consistent formal charge of +0.3, this means that there are 0.48 electrons remaining to take part in the interstitial conduction. An integration over the boron states lying just below and just above the Fermi level yields a value of 0.16 electrons contributed by the boron to the conduction group but the boron has, overall, 3.3 electrons. The B  $2s$  population is 1.1 and so, adding one  $p$ -electron, 2.1 electrons can be considered as taking part in the B–B bonding in the zig-zag chains. Hence, overall, we can write the formula for the configuration of an FeB unit in the crystal as in Table 4. Using the magnetic-moment data given in Lundquist *et al.* [12], we can partition the electrons in a similar way for CoB and MnB. The lower number of conduction electrons found in FeB compared with iron itself helps to explain the lower specific electrical conductivity of this material.

The case of NiB is now easy to understand: earlier we showed that the  $d$  sub-band was almost full, the holes left in it amounting to only about 0.2 electrons. The experimental observation by Lundquist [12] is that NiB is very weakly paramagnetic and this was attributed by these workers to a lack of holes in the  $d$  band. We now bear this out by direct calculation. Again, we draw attention in passing to the very high  $d$ -orbital populations calculated for these binary materials. It should be noted that, in a formal sense, one is talking about  $Fe^{3+}$ ,  $Co^{3+}$ , and  $Mn^{3+}$  and these would have formal  $d$  configurations of  $d^5$ ,  $d^6$  and  $d^4$ .

The Mössbauer isomer shift has been measured for FeB by Cooper *et al.* [6] as  $0.28 \text{ mm sec}^{-1}$ . This positive shift with respect to metallic iron shows that, in FeB, there is a decrease in  $s$ -electron density at the iron nucleus. This is clearly found in the calculations, where the  $s$ -electron population is very considerably decreased and, hence, the  $s$ -electron density at the nucleus. An increase in the

**Table 4.** Partition of Electrons in MnB, FeB, and CoB

	Localized $3d$	Itinerant $3d$	Conduction electrons	Boron configurations
MnB	2.0	3.79	0.72	$2p^{1.36}(s^{1.13}p^{1.0})$
FeB	7.0	0.22	0.64	$2p^{1.04}(s^{1.10}p^{1.0})$
CoB	8.0	0.49	0.63	$2p^{0.78}(2s^{1.10}p^{1.0})$

**Table 5.** Bonding patterns in the monoborides from a  $M_{16}B_{16}$  cluster calculation. The highest energy electrons are allowed to diffuse into vacant orbitals having higher energy a) 0.01 eV, and b) 0.1 eV

$M_{16}B_{16}$ Bond Indices	$M-\Sigma M_{\text{perp}}$	$M-\Sigma M_{\text{plan}}$	$B-\Sigma M_{\text{perp}}$	$B-\Sigma M_{\text{plan}}$	$B-\Sigma B_{\text{perp}}$	$B-\Sigma B_{\text{plan}}$
<b>M = Ti</b>						
ground state	1.838	0.992	0.931	0.793	2.126	0.063
a) 0.01 eV	1.679	0.913	0.927	0.797	2.152	0.063
b) 0.1 eV	1.612	0.472	0.912	0.796	2.159	0.063
<b>M = Mn</b>						
ground state	2.530	1.532	1.032	0.906	1.544	0.145
a) 0.01 eV	2.254	1.006	1.035	0.901	1.544	0.146
b) 0.1 eV	0.683	0.385	1.007	0.901	1.558	0.151
<b>M = Fe</b>						
ground state	1.917	0.946	0.916	0.832	1.336	0.161
a) 0.01 eV	1.201	0.622	0.911	0.836	1.336	0.161
b) 0.1 eV	0.611	0.348	0.896	0.830	1.343	0.163
<b>M = Co</b>						
ground state	0.670	0.373	0.782	0.728	0.961	0.182
a) 0.01 eV	0.662	0.368	0.780	0.724	0.964	0.331
b) 0.1 eV	0.418	0.217	0.785	0.735	0.997	0.330

number of *d*-electrons over the metal, as is found, also leads to an enhancement of the Mössbauer shift.

### 3.5. Cluster Calculations

The results of cluster calculations, obtained as previously described, are now discussed. The bond index was calculated for each definite interaction in the supercell and, as has been shown previously [5], the bond index can be directly correlated with the strength of the relevant bond. Hence, it is of some interest to determine which are the strong bonds in the structure and which bonds are affected when the central element changes or when electrons are excited into the conduction band. Table 5 shows the bond indices in the series of unit cells generated by the “unexcited” crystal and the crystal where excitations of 0.01 eV and 0.1 eV are allowed. At 300 K, levels lying 0.01 eV above filled levels will be 68% populated whilst those lying 0.1 eV above will be only 2% populated. The first interesting comparison is that between the ground states of the systems: B–B planar bonding (in the *xy* plane) is never very important in any of the borides, whereas B–B perpendicular bonding is clearly very strong in a covalent sense and, indeed, in titanium boride it has the nature of a double bond throughout the crystal. This particular bonding declines from the titanium down to cobalt but even at cobalt, the B–B zig-zag bond in the *z* direction has the dimensions of a single bond. The boron metal bonding is, clearly quite important and, as defined in the cluster calculation, is a covalent bond. One notices that the boron metal bonding is similar, independent of whether the metal lies in the same plane or is perpendicular to the boron.

Metal–metal bonding is, obviously, of some importance in these boride crystals and it is interesting that this type of bonding running parallel with the boron chains is much more important than that in the directions orthogonal to this. It is interesting that this particular type of bonding rises from titanium to a maximum in manganese and then declines towards cobalt. This happens because the *d* band is being filled and the maximum number of bonding electrons is present at manganese and, as the *d* band fills in the iron and cobalt electronic structures, more antibonding interactions are included, which reduces the metal–metal bond orders and, hence, the bond indices between the metals.

When we consider the crystals in which electrons have been excited into higher levels, then some interesting and dramatic features are found. Firstly, it is noticeable that the boron–boron and boron–metal bonding is almost unaffected by excitation of electrons. However, the metal–metal bonding is, in all cases, drastically weakened by the excitation effect. This means that heating of the crystal will lead, firstly, to a drastic decrease in the forces by which the metal atoms are held into the lattice and, hence, the onset of disorder among the metal atoms in the lattice will be effective under milder conditions than that required to break up the boron–boron sub-lattice.

*Acknowledgement.* One of us (E.A.C.) thanks the Royal Society and the Academia Científica A.C. (México) for a grant.

## References

1. Armstrong, D. R., Breeze, A., Perkins, P. G.: *J. Physics. C, Solid State Physics* **8**, 3558 (1975)
2. Armstrong, D. R., Breeze, A., Perkins, P. G.: *J. Chem. Soc. (Lond.) Faraday II Trans.* **73**, 952 (1977)
3. Armstrong, D. R., Perkins, P. G.: *J. Chem. Soc. (Lond.) Faraday II Trans.* **75**, 12 (1979)
4. Armstrong, D. R., Perkins, P. G., Stewart, J. J.: *J. Chem. Soc. (Lond.) Dalton Trans.*, 838 (1973)
5. Bell, T. N., Perkins, P. G.: *J. Phys. Chem.* **81**, 2102 (1977)
6. Cooper, J. D., Gibb, T. C., Greenwood, N. N., Parish, R. V.: *Trans. Faraday Soc.* **60**, 2097 (1964)
7. Hoffmann, R.: *J. Chem. Physics* **39**, 1397 (1963)
8. Johnson, O.: *Bull. Chem. Soc. Japan* **45**, 1599 (1972) *ibid* **46**, 1919, 1923 (1973)
9. Joyner, D. J., Johnson, O., Hercules, D. M.: *J. Am. Chem. Soc.* **102**, 1910 (1980)
10. Joyner, D. J., Johnson, O., Hercules, D. M.: *Private Communication* (1979)
11. Lundstrom, T.: *Arkiv for Kemi* **31**, 227 (1969)
12. Lundquist, N., Myers, H. P., Western, R.: *Phil. Mag.* **7**, 1187 (1962)
13. Marwaha, A. K., Perkins, P. G., Stewart, J. J.: *Theoret. Chim. Acta (Berl.)* **59**, 555 (1981)
14. Marwaha, A. K., Perkins, P. G., Stewart, J. J.: *Theoret. Chim. Acta (Berl.)*. **59**, 569 (1981)
15. Mattheis, L. F.: *Phys. Rev.* **B5**, 290, 306 (1972)
16. Perkins, P. G., Stewart, J. J.: *J. Chem. Soc., (Lond.) Faraday II Trans.* **76**, 520 (1980)

Received February 22, 1983